Chemical Engineering Journal 155 (2009) 241–247

Contents lists available at ScienceDirect

Chemical Engineering Journal

journal homepage: www.elsevier.com/locate/cej

Kinetic study of three-way catalyst of automotive exhaust gas: Modeling and application

Li-Ping Ma[a,*], Hans-Jörg Bart[b], Ping Ning[a,b], Aimin Zhang[c], Guozheng Wu[a], Zhu Zengzang[c]

[a] Department of Environmental Science and Engineering, Kunming University of Science and Technology, 63 Wenchang Rd, 12-1 Street, 650093 Kunming, China
[b] Lehrstuhl für Thermische Verfahrenstechnik, TU Kaiserslautern, D-67653 Kaiserslautern, Germany
[c] Kunming Sino-Platinum Metals Catalyst Co. Ltd., 650041 Kunming, China

ARTICLE INFO

Article history:
Received 20 May 2008
Received in revised form 13 July 2009
Accepted 24 July 2009

Keywords:
Kinetics
Three-way catalyst
Mathematical model
Elementary reaction steps
Oxidation
Reduction

ABSTRACT

The kinetics of carbon monoxide and propylene oxidation as well as nitrous oxide reduction on a Pd–Rh catalyst were determined with synthetic gas mixtures between 500 and 700 K. The overall reaction rate expression was constructed from elementary reaction steps and the kinetic parameters were determined from the experiments. A transient mathematical model has been developed to simulate automobile exhaust gas conversion based on the kinetics model equations. A comparison of simulated results with engine experiments proved to be successful. Results indicate that the reaction mechanisms proposed in this study are capable to describe the behavior of automotive exhaust gas converters, if mutual interactions of gaseous components and surface species are taken into account via elementary kinetic steps.

1. Introduction

Noble metal catalysts have received considerable attention for more than 20 years for used in automotive emission control systems [1–4]. Most efforts were laid on the effect of physical processes (heat and mass transfer processes at channel and monolith scale, flow distribution, etc.) [5–9], and modeling of the chemical reaction in the three-way converter [10–13]. As state of the art, theoretical predictions and comparisons with experiments are usually made based on the rate expressions provided by Voltz et al. [14], which accounts for oxidation of CO, H_2 and of a single lumped hydrocarbon in a lean exhaust gas. However, it is known that the three-way catalyst has been further optimized and had got great improvement with the high requirement of exhaust gas emission control and therefore reactions other than those mentioned previously take place [15–17]. The exhaust gas contains several types of hydrocarbon which have different effects on monolith behavior such as NO reduction, oxygen storage in ceria, water–gas shift reaction, etc. [18–20].

When accounting for the new catalyst and the new reactions, the main problem is the lack of kinetic data or the need for time-consuming experimental investigations. Moreover, these experiments should be performed for any new catalyst. Kunming Sino-Platinum Metals Catalyst Co. Ltd. is responsible to advance three-way catalyst technology in China, a series of commercial converters which meet the emission limits of Europe III and Europe IV have been developed and satisfying results had been got by the company. However, the basic kinetic data is lacking for developing a three-way catalytic converter. The aim of this paper is to research the kinetics of carbon monoxide, hydrocarbon oxidation and NO reductions reaction on the new catalyst developed in order to reasonably design the converter. The reaction kinetics chemistry is presented and validated with experiments obtained from an engine on a bench test. A mathematical model has been developed which describes the dynamic behavior of a monolith catalytic converter for examining how the light-off behavior of a catalyst monolith is influenced by properties, such as the poison penetration depth and the location and width of the noble metal band.

2. Mechanism and methods

2.1. Chemical reaction kinetics of automobile exhaust gas

The time-resolved composition of a real exhaust gas with respect to hydrocarbons is known from analysis which lumps together all the hydrocarbons. A more detailed composition is available only from a chromatographic analysis on the whole amount of gas collected during an experiment. This poor knowledge of the composition makes it necessary to assume firstly that the exhaust gas has a constant average composition with respect to hydrocarbon.

* Corresponding author. Tel.: +86 871 5170905; fax: +86 871 5170906.
E-mail address: lipingma22@hotmail.com (L.-P. Ma).

1385-8947/$ – see front matter.
doi:10.1016/j.cej.2009.07.045

Nomenclature

C_{Tg}	total concentration in the bulk gas phase (mol m^{-3})
C_j	concentration of species i in the bulk gas phase (%)
c_{pg}	heat capacity of gas (J kg^{-1} K^{-1})
c_{ps}	heat capacity of catalyst (J kg^{-1} K^{-1})
D_h	monolith radial coordinate (m)
D_T	diameter of monolith channel (m)
h_D	mass transfer coefficient of gas (m s^{-1})
h	heat transfer coefficient (W m^{-2} K^{-1})
ΔH	heat of reaction (kJ kmol^{-1})
r	reaction rate (mol s^{-1} m^{-3})
R_j	whole reaction rate of species j
S_{cat}	catalytic surface area per unit catalyst volume (m^2 m^{-3})
T_g	temperature of gas (°C)
T_a	temperature of environment (°C)
T_s	temperature of the surface of catalyst (°C)
t	time (s)
u	axial gas velocity (m s^{-1})

Greek letters

ε	surface roughness
ρ	density (kg m^{-3})

Superscripts

*	at equilibrium

Subscripts

i, j	compound index of gas
g	gas
s	solid
in	gas inlet

Secondly, it requires to account for families of hydrocarbon which induce specific behaviors. We have chosen four typical reactions which includes oxidizing reaction of carbon monoxide (1), C_3H_6 (3), reduction of NO (4) and water–gas shift reaction (2). The corresponding reactions are shown in Table 1 and the heat of reaction at the expected temperature can be calculated according to the Gibbs energy equation through the standard state heat of reaction $\Delta H(298\,K)$ [21].

The kinetic scheme used in the simulations, was taken from various literature sources that presented kinetics based on elementary steps for the reactions of interest. These reactions were studied on different noble metal catalyst, such as Pt and Rh, supported by either silica or alumina. As a major incentive of this work is to explore the interaction and competition of the individual global reactions in a simulative automotive exhaust gas mixture. Such interaction is expressed by elementary reaction steps via common reactants, intermediates and surface species based on Langmuir–Hinshelwood type, which allows to clarify the interactions between the various reacting species via common surface intermediates. The steps involving CO and NO were taken from literature [15,18]. The elementary step reactions for propylene oxidation are very complex and not available in the literature. Based on collision theory, it is supposed that firstly C_3H_6 was decomposed into two intermediates (P_1^*, R^*) and then were separated into CH_2^* or CH_3^* ($2R^*$), which finally react with adsorbed oxygen atoms to produce CO_2 and H_2O. The elementary reactions and the reaction pathways are then as follows, where σ indicates adsorption sites or adsorbed species:

Table 1
Basic reaction.

Reactions	$\Delta H(298\,K)$ (kJ mol^{-1})
(1) $CO + 2O_2 \rightarrow 2CO_2$	−676.51
(2) $CO + H_2O \rightarrow CO_2 + H_2$	−41.16
(3) $C_3H_6 + (9/2)O_2 \rightarrow 3CO_2 + 3H_2O$	−1820.27
(4) $CO + NO \rightarrow CO_2 + N_2$	−373.36

(1) Oxidation of CO:

$$CO + \sigma \rightleftharpoons CO^* \quad (a)$$

$$O_2 + 2\sigma \rightleftharpoons 2O^* \quad (b)$$

$$CO^* + O^* \rightarrow CO_2 + 2\sigma \quad (1)$$

(2) Water–gas reaction with CO:

$$H_2O + \sigma \rightleftharpoons H_2O^* \quad (c)$$

$$H_2O^* + \sigma \rightleftharpoons HO^* + H^* \quad (d)$$

$$2H^* \rightarrow H_2 + 2\sigma \quad (2)$$

$$CO^* + OH^* \rightarrow CO_2 + \sigma + H^* \quad (3)$$

(3) Oxidation of hydrocarbon:

$$P + \sigma \rightleftharpoons P^* \quad (e)$$

$$P^* + \sigma \rightleftharpoons P_1{}^* + R^* \quad (f)$$

$$P_1{}^* + \sigma \rightleftharpoons 2R^* \quad (g)$$

$$R^* + 3O^* \rightarrow CO_2 + H_2O^* + 2\sigma \quad (4)$$

(4) Reaction of NO with CO:

$$NO + \sigma \rightleftharpoons NO^* \quad (h)$$

$$CO^* + NO^* \rightarrow CO_2 + N^* + \sigma \quad (5)$$

$$2N^* \rightarrow N_2 + 2\sigma \quad (6)$$

The fraction of vacant surface sites follows from:

$$\theta_{CO}+\theta_P + \theta_{P1} + \theta_R + \theta_O + \theta_{OH} + \theta_{H_2O} + \theta_H + \theta_{NO} + \theta_N + \theta_V = 1 \quad (7)$$

In each reaction path from (a) to (h), the steady-state continuity equations for the surface species CO^*, O^*, NO^*, $C_3H_6{}^*$, H_2O^*, H^* are supposed to be in equilibrium. Therefore:

$$K_{CO} = \theta_{CO}/(C_{CO}\theta_V) \Rightarrow \theta_{CO} = K_{CO}C_{CO}\theta_V \quad (8)$$

$$K_O = \theta_O{}^2/(C_{O2}\theta_V{}^2) \Rightarrow \theta_O = (K_O C_{O2})^{1/2}\theta_V \quad (9)$$

$$K_{H2O} = \theta_{H2O}/(C_{H2O}\theta_V) \Rightarrow \theta_{H2O} = K_{H2O}C_{H2O}\theta_V \quad (10)$$

$$K_P = \theta_P/(C_P\theta_V) \Rightarrow \theta_P = K_P C_P \theta_V \quad (11)$$

$$\theta_{P1} = K_{P1}K_R{}^{-1/3}C_P{}^{2/3}\theta_V \quad (12)$$

$$K_R = \theta_R{}^3/(C_P\theta_V{}^3) \Rightarrow \theta_R = K_R{}^{1/3}C_P{}^{1/3}\theta_V \quad (13)$$

$$K_{NO} = \theta_{NO}/(C_{NO}\theta_V) \Rightarrow \theta_{NO} = K_{NO}C_{NO}\theta_V \quad (14)$$

While for the reaction from (1) to (6), the reaction rate can be expressed as follows:

$$r_1 = k_1\theta_{CO}\theta_O \quad (15)$$

$$r_2 = k_2\theta_{CO}\theta_{OH} = k_H\theta_H{}^2 \quad (16)$$

$$r_3 = k_3\theta_R\theta_O{}^3 \quad (17)$$

$$r_4 = k_4\theta_{CO}\theta_{NO} = k_N\theta_N{}^2 \quad (18)$$

From Eqs. (10), (16), (17) and (18) there is

$$\theta_H = (k_2 K_{OH} K_{CO} C_{CO} C_{H2O}/k_H)^{1/3}\theta_V$$

$$\theta_{OH} = {k_H}^{1/3} {K_{OH}}^{2/3} {C_{H2O}}^{2/3} (k_2 K_{CO} C_{CO})^{-1/3}\theta_V$$

$$\theta_N = (k_4 K_{CO} K_{NO} C_{CO} C_{NO}/k_N)^{1/2}\theta_V$$

$$\begin{aligned}\theta_V = {} & 1/(K_{CO}C_{CO} + K_P C_P + K_{P1}{K_R}^{-1/3}{C_P}^{2/3} + {K_R}^{1/3}{C_P}^{1/3} \\ & + (K_O C_{O2})^{1/2} + {k_H}^{1/3}{K_{OH}}^{2/3}{C_{H2O}}^{2/3}(k_2 K_{CO} C_{CO})^{-1/3} \\ & + K_{H2O}C_{H2O} + (k_2 K_{OH} K_{CO} C_{CO} C_{H2O}/k_H)^{1/3} + K_{NO}C_{NO} \\ & + (k_4 K_{CO} K_{NO} C_{CO} C_{NO}/k_N)^{1/2} + 1) = 1/G\end{aligned}$$

The rate expression of these reactions on the catalyst is then:

$$\begin{aligned}r_1 &= k_1 K_{CO} {K_O}^{1/2} C_{CO} {C_{O2}}^{1/2}/G^2 = \bar{k}_1 C_{CO} {C_{O2}}^{1/2}/G^2 \\ &= k_{01}\, e^{-E/RT} C_{CO} {C_{O2}}^{1/2}/G^2 \end{aligned} \quad (19)$$

$$\begin{aligned}r_2 &= (k_2 K_{CO} C_{CO} K_{OH} C_{H2O})^{2/3} {k_H}^{1/3}/G^2 = \bar{k}_2 {C_{CO}}^{2/3} {C_{H2O}}^{2/3}/G^2 \\ &= k_{02}\, e^{-E/RT} {C_{CO}}^{2/3} {C_{H2O}}^{2/3}/G^2 \end{aligned} \quad (20)$$

$$\begin{aligned}r^3 &= k_3 {K_R}^{1/3} {C_P}^{1/3} {K_O}^{3/2} {C_{O2}}^{3/2}/G^4 = \bar{k}_3 {C_{O2}}^{3/2} {C_P}^{3/2}/G^4 \\ &= k_{03}\, e^{-E/RT} {C_{O2}}^{3/2} {C_P}^{1/3}/G^4 \end{aligned} \quad (21)$$

$$r^4 = k_4 K_{CO} K_{NO} C_{CO} C_{NO}/G^2 = \bar{k}_4 C_{CO} C_{NO}/G^2 = k_{04}\, e^{-E/RT} C_{CO} C_{NO}/G^2 \quad (22)$$

where

$$\begin{aligned}G = {} & K_{CO}C_{CO} + K_P C_P + K_{P1}{K_R}^{-1/3}{C_P}^{2/3} + {K_R}^{1/3}{C_P}^{1/3} + (K_O C_{O2})^{1/2} \\ & + {k_H}^{1/3}{K_{OH}}^{2/3}{C_{H2O}}^{2/3}(k_2 K_{CO} C_{CO})^{-1/3} + K_{H2O}C_{H2O} \\ & + (k_2 K_{OH} K_{CO} C_{CO} C_{H2O}/k_H)^{1/3} + K_{NO}C_{NO} \\ & + (k_4 K_{CO} K_{NO} C_{CO} C_{NO}/k_N)^{1/2} + 1 \\ = {} & K_{a1}C_{CO} + K_{a2}C_P + K_{a3}{C_P}^{2/3} + K_{a4}{C_P}^{1/3} + K_{a5}{C_{O2}}^{1/2} \\ & + K_{a6}{C_{H2O}}^{2/3}{C_{CO}}^{-1/3} + K_{a7}C_{H_2O} + K_{a8}(C_{H2O}C_{CO})^{1/3} \\ & + K_{a9}C_{NO} + K_{a10}(C_{CO}C_{NO})^{1/2} + 1 \end{aligned} \quad (23)$$

The reaction rate for the different components in the exhaust gas could be written as:

$$R_{CO} = r_1 + r_2 + r_4 \quad (24)$$

$$R_{O2} = r_1 + r_3 \quad (25)$$

$$R_{HC} = r_3 \quad (26)$$

$$R_{NO} = r_4 \quad (27)$$

where R_j represents the whole reaction rate for each component on the catalyst, r means the reaction control rate of each reaction pathway (Table 1), K is the adsorption equilibrium constant, C_i represents the concentration of a species i (CO, H_2O, ...) and k_i is the reaction rate constant.

2.2. Mathematical model of the catalytic converter

It is desirable to extend the kinetic model to monolith catalytic converter for reasonable designing of converter. Mathematical modeling is an important method for researching and designing a catalytic converter. Some studies mainly focused on physical process (mass and heat physics transfer) at channel and monolith scale, while others focused on predicting the conversion behaviors of catalytic converters and their design optimisation [2–4,10], they had studied the mathematical modeling of heat and mass transfer in exhaust system of a cold-start engine and obtained good agreement between measure and calculated. Based on previous works, a mathematical model has been developed to describe the dynamic behavior of a three-way catalytic converter during its warm-up period considering of upwards kinetic hypothesis. In the early stage of a warming-up at the engine cold start there are no chemical reaction in the converter. When the monolith temperature reaches a range of 250–340 °C (the light-off temperature window), the reaction starts and the converter is in the activated state. The mathematical model is based on following assumptions:

(1) Pelect number of tail gas usually is large enough, so the axial heat conduction and diffusion is neglected.
(2) The flow in every cell channel is plug-flow.
(3) Gas temperatures and concentrations are identical for all cell channels.
(4) When the monolith temperature reaches the light-off temperature, chemical reactions occur and the reaction heat is considered, otherwise, the catalyst is known to be non-activated.

The energy balance is for the gas phase:

$$\delta\rho_g \cdot c_{pg}\frac{\partial T_g}{\partial t} = -\rho_g \cdot u \cdot c_{pg}\frac{\partial T_g}{\partial x} + h \cdot S(T_s - T_g) \quad (28)$$

and for the solid phase:

$$\begin{aligned}(1-\delta)\cdot\rho_s \cdot c_{ps}\frac{\partial T_s}{\partial t} = {} & (1-\delta)\cdot\lambda_s \cdot \frac{\partial^2 T_s}{\partial x^2} + h \cdot S \cdot (T_g - T_s) \\ & + S_{cat}\sum_{j=1}^{5}(-\Delta H_j)\cdot R_j \end{aligned} \quad (29)$$

where S_{cat} is the catalytic surface area per unit catalyst volume, S is the geometric surface area per unit catalyst volume. Without reactions, the last term in Eq. (29) equals 0.

The mass balance of the catalytic converter is for the gas phase:

$$\frac{\partial c_{gj}}{\partial t} = -u\frac{\partial c_{gj}}{\partial x} - k_{Dj}\cdot S\cdot(c_{gj} - c_{sj}) \quad (30)$$

and the solid phase:

$$S_{cat}\cdot R_j = \frac{\rho_g}{M}\cdot k_{Dj}\cdot S\cdot(c_{gj} - c_{sj}) \quad (31)$$

The heat transfer and mass transfer coefficients are:

$$h = \frac{Nu\,\lambda_g}{d} \quad (32)$$

and

$$k_{Dj} = \frac{Sh\cdot D_j}{d} \quad (33)$$

where D_j is the diffusivity of species j and is obtained from Slattery-Bird [22].

The boundary condition for the catalyst monolith are as follows:

$$\begin{cases} T_g(0,t) = T_g^{in} \\ c_{gj}(0,t) = c_j^{in} \end{cases} \qquad \frac{dT_s}{dx}(L,t) = \frac{dT_s}{dx}(0,t) = 0 \quad (34)$$

$$T_s(x,0) = T_a \quad (35)$$

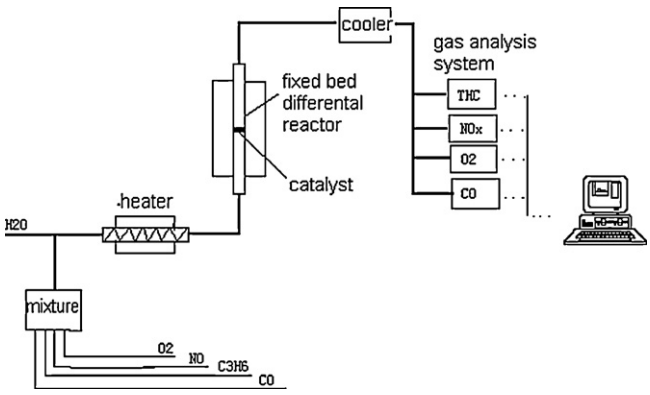

Fig. 1. Kinetic experimental apparatus.

3. Experimental

3.1. Catalyst preparation

The catalytic activity of a catalyst is determined by its structure and chemical composition. The method for catalyst preparation may seriously affect its physical and chemical characteristics such as surface area, pore structure, crystalloid and catalytic structure. A powder catalyst, which contained 1.6% noble metal (Pd:Rh = 5:1), was firstly prepared by impregnating Pd using a non-aqueous method on γ-Al_2O_3. After impregnation, the catalysts were dried overnight at 120 °C and calcined in air at 500 °C for 5 h. Secondly, that catalysts impregnated with Pd were further impregnated with Rh and then dried overnight at 120 °C and calcined in air at 500 °C for 5 h. After that, the catalysts used in this study have the following characteristics: BET surface area (BET) = 138.7 m^2/g; total pore volume (TPV) = 0.2631 cc/g; average pore size (APS) = 3.79 nm and mass density = 0.8095 g/ml.

3.2. Experimental setup

The apparatus for kinetic experiments, shown in Fig. 1, consisted of three sections: a gas-blending system, the catalytic reactor and an analytical instrumentation. The desired concentration of reactant gases were obtained by blending pure CO, C_3H_6, O_2, NO, and N_2 (balance gas). The synthetic gas mixture was passed through a electrically thermostated bubble column (a control temperature is 120 °C to humidity the gas at a desired level) and then through heated lines to the reactor. The differential reactor was constructed of stainless steel tubing (10 mm i.d. and 500 mm in length) and controlled by a thermocouple placed near the center of the bed. The desired amounts of catalyst was placed in the reactor and a Cr–Al thermocouple was positioned in the catalyst bed. The composition of the inlet gas was determined and then the gas was passed over the catalyst, which was maintained at the desired temperature and space velocities of 40,000 h^{-1}. 0.05 g catalysts with particle size 1.0 μm were used. The concentrations of inlet gas and analysis methods are listed in Tables 2 and 3. The engine test bed facility system is a fully instrumented 491 engine carried with a TWC produced by Kunming Sino-Platinum Metals Catalyst Co. Ltd. The engine is a 4-stoke, speed 2900 rpm, velocity 4000 ± 500 h^{-1}, open rate of petrol door 32%.

Table 2
Concentration of reactant gas and the analysis method.

Gas	Concentration (vol%)	Analysis method
CO	1.0–2.0	QGS-08B
C_3H_6	6×10^{-4} to 1.4×10^{-3}	DANI THM411 hydrocarbons controller
O_2	0.8–1.5	QZS-9601
H_2O	10–15	
NO	5×10^{-4} to 1.0×10^{-3}	ML9841A NO_x analysis
N_2	Equilibrium gas	

Table 3
Inlet gas concentration (300 °C).

	CO (%)	THC (ppm)	NO (ppm)	O_2 (%)	λ
1	2.0	1400	1000	1.42	0.9
2	1.8	1200	900	1.40	1
3	1.5	1000	800	1.16	1
4	1.3	800	700	0.98	1
5	1.0	600	500	0.82	1.1

$\lambda = (C_{NO} + 2C_{O2})/(C_{CO} + 9C_{C3H6})$.

4. Results and discussion

One of the key objectives of this study was to develop a kinetic model which describes the reaction process leading to a real engine exhaust gas. The experimental data for the oxidations and reduction reactions in the synthetic gas mixtures were used to test various reaction mechanisms and associated kinetic rate equations and develop suitable equations to be incorporated into a complete catalytic converter.

In a differential reactor the conversion of reactants in the bed is extremely small. That means, the reactor is considered to be gradient-less and reaction rate is considered spatially uniform within the bed. The reaction rate is calculated as follows:

$$(-R_A) = \frac{Q}{V_R}(C_{AF} - C_{AO}) \tag{36}$$

where $-R_A$ is the reaction rate explained as equation from (24) to (27), and the reactant concentration is $(C_{AF} + C_{AO})/2$. Q is the volume rate of reactant.

At a given temperature the concentration of inlet gases is adjusted. The next step is to evaluate the reaction rate constants. At a given input the minimal error in the calculated outlet concentrations result from the best parameter set obtained in a optimization procedure.

After minimization using Maple 10, the adsorption equilibrium constant from K_{a1} to K_{a10} and k_1 have been evaluated. The same method was also used for Eqs. (20), (21) and (22).

A change of the temperature from 573 to 598, 623, 648 until 673 K using this method allows the determination of the adsorption equilibrium constants at different temperatures. According to the Van't Hoff equation, the adsorption equilibrium constant in Eq. (23) can be calculated as to:

$$K_{aj} = K_{a0j} \exp\left(\frac{-\Delta H_{aj}}{RT_s}\right) \tag{37}$$

where ΔH_{aj} and pre-exponential adsorption factor K_{a0j} of each reaction can be got from a logarithmic plot of Eq. (37) with experiment data at different temperatures which were listed in Table 4.

The kinetic constants $\bar{k}_j$ in Eqs. (19)–(22) could be derived using the Arrhenius equation at different temperatures:

$$\bar{k}_j = k_{0j} \exp\left(-\frac{E_{aj}}{RT_s}\right) \tag{38}$$

and expression (38) is equivalent to

$$\ln(\bar{k}_j) = \ln(k_{0j}) - \frac{E_{aj}}{RT_s} \tag{39}$$

According to Arrhenius equation (38), the reaction rate constant in equation can be calculated as shown in Fig. 2 and listed in Table 5. The reaction rate equations of CO, O_2, C_3H_6 and NO are

Table 4
Adsorption constants.

Constant	Adsorption heat, ΔH_a (J mol^{-1})	Adsorption factor, K_{a0j}
K_{a1}	-2.423×10^5	2.728×10^{-20}
K_{a2}	57265.2	1.1204×10^9
K_{a3}	-1.252×10^5	2.487×10^{-9}
K_{a4}	7346.5	100.38
K_{a5}	−68184.78	1.481×10^{-5}
K_{a6}	1.783×10^4	8769.19
K_{a7}	3.219×10^4	3.819×10^5
K_{a8}	1.231×10^5	1.361×10^{13}
K_{a9}	-1.199×10^5	7.509×10^{-7}
K_{a10}	-2.775×10^5	1.252×10^{27}

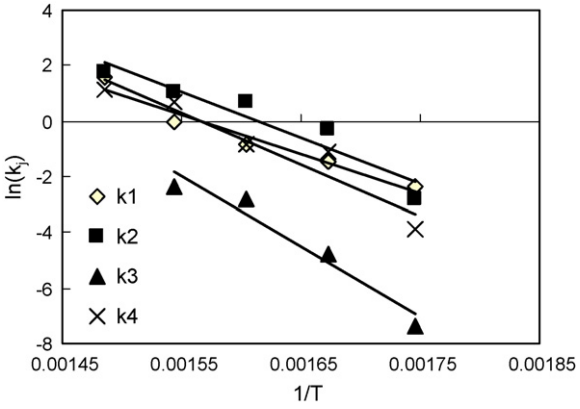

Fig. 2. The relationship between log $(1/T)$–log(k_j) for different kinetic constants.

Table 5
Reaction rate constants.

Rate constant	E_j (J mol^{-1})	K_{0j}
$\bar{k}_1$	1.061×10^5	7.573×10^9
$\bar{k}_2$	1.289×10^5	5.037×10^{11}
$\bar{k}_3$	1.211×10^5	1.392×10^{12}
$\bar{k}_4$	1.517×10^5	4.092×10^{14}

then expressed as follows:

$$R_{CO} = 7.573 \times 10^9\, e^{(-12{,}759/Ts)} C_{CO} {C_{O2}}^{1/2}/G^2 + 5.037 \times 10^{11}\, e^{(-15{,}513/Ts)} {C_{CO}}^{2/3} {C_{H2O}}^{2/3}/G^2 + 4.092 \times 10^{14}\, e^{(-18{,}259/Ts)} C_{CO} C_{NO}/G^2 \quad (40)$$

$$R_{O2} = 7.573 \times 10^9\, e^{(-12{,}759/Ts)} C_{CO} {C_{O2}}^{1/2}/G^2 + 1.392 \times 10^{12}\, e^{(-14{,}571/Ts)} {C_{O2}}^{3/2} {C_P}^{1/3}/G^4 \quad (41)$$

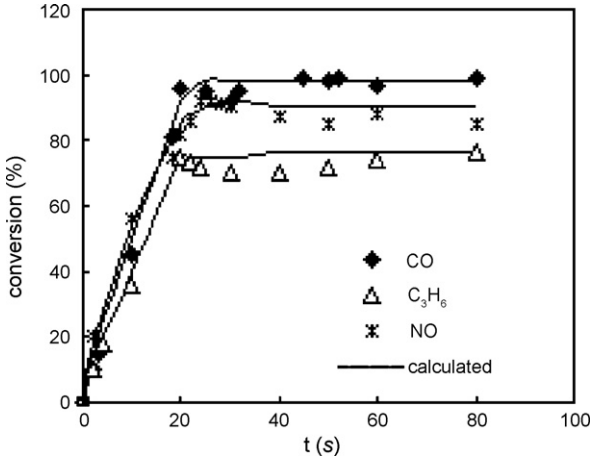

Fig. 3. Comparison of experimental and simulated results of the average conversion of CO, NO and C_3H_6.

$$R_{HC} = 1.392 \times 10^{12}\, e^{(-14{,}571/Ts)} {C_{O2}}^{3/2} {C_P}^{1/3}/G^4 \quad (42)$$

$$R_{NO} = 4.092 \times 10^{14}\, e^{(-18{,}259/Ts)} C_{CO} C_{NO}/G^2 \quad (43)$$

The reliability of the kinetic description can be checked by comparing simulation results to experiments with complex mixtures. The parameters used in calculation are listed in Table 6. A detail description of the numerical technique used to solve Eqs. (28)–(31) is given in an earlier paper [23].

Fig. 3 compares the experimental and simulated results of the average conversion of CO, NO and C_3H_6. It can be seen that the time history of the emissions are reasonably simulated. During the cold start (first 25 s), the catalyst has not been activated and no reactions happened, the exhaust concentration is as the same as the input. With the gas temperature upswing, the catalyst is activated and reactions take place. The exhaust concentration descended gradually, which can be noted from calculated and measured results. 60 s later after starting, the exhaust concentration arrived at the stable value and the catalytic converter has come to a stable working period. The conversion of CO, NO and C_3H_6 almost arrived 98%, 90% and 80%, respectively.

The application of the kinetic model for real engine exhaust at cold start is illustrated in Figs. 4 and 5. The experiment had been done using the bench test equipment which had been explained above. It was indicated (Fig. 4) that after starting the engine, the outlet temperature rose quickly from 300 to 800 K and then fluctuated around 800 ± 150 K. The fluctuation of the outlet temperature could be mainly due to the experiment cycle and variation of A/F ratio. During the experiment, in order to simulate the practical operation of a car, the engine was operated in a cycle in which fuel (gasoline) was firstly supplied for 60 s and then cut off for 5 s. During the first 60 s of fuel supplying, the outlet temperature rose a little, while during the 5 s of fuel deprivation, the outlet temperature declined a little. Also, variation of A/F ratio could inevitably make

Table 6
Simulation parameters.

Parameters	Amount	Parameters	Amount
Specific heat of gas, c_{pg} (J kg^{-1} K^{-1})	1091	Density of gas, ρ_g (kg m^{-3})	0.903
Density of solid, ρ_s (kg m^{-3})	2500	Thermal conductivity, λ_s (W m^{-1} K^{-1})	1.675
Substrate length, z (m)	0.10	Pipe length, L (m)	1.0
Hydraulic diameter of monolith cell channel, d (m)	0.001	Pipe inner diameter, $d1$ (m)	0.05
Pipe outer diameter, $d2$ (m)	0.056	Axial gas velocity, u (m s^{-1})	1.1
Pipe thermal diffusivity, α (m^2 s^{-1})	1.315×10^{-5}	Surface roughness, ε	0.1
Time step, Δt (ms)	5	Axial space step of cell channel, Δx (m)	0.002

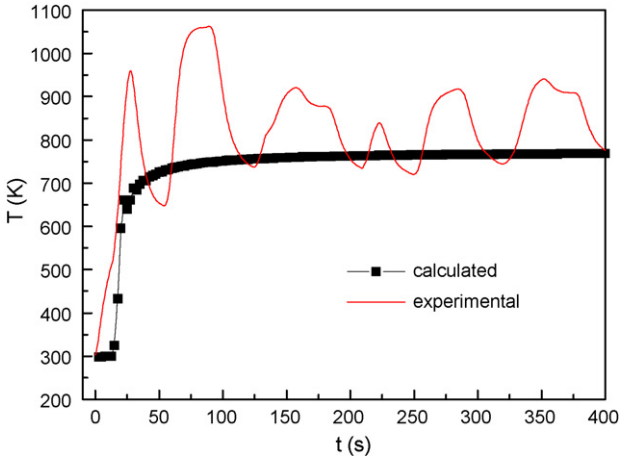

Fig. 4. Comparison of exhaust gas temperature at exhaust of converter by calculating with experiment.

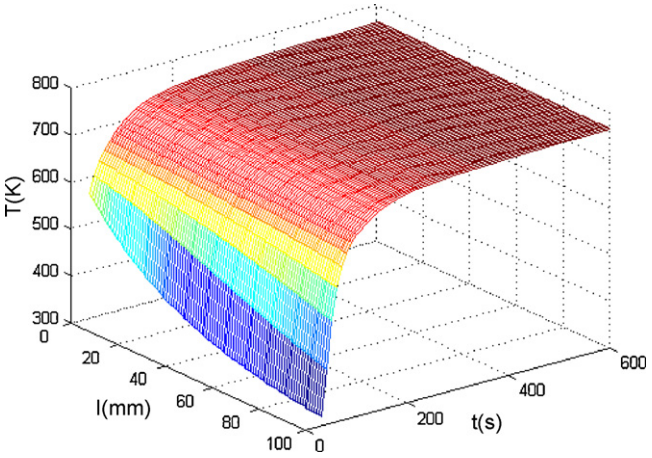

Fig. 6. The temperature distribution of gas phase in the converter at different time by modeling.

a contribution to the fluctuation of outlet temperature. The model well predicts the general trend of the measured experimental data.

Fig. 5 compares the predicted concentrations of CO, HC and NO at the outlet of converter with measured data. It is noted (Fig. 5(a)) that the results of calculation is in coincidence with the measured ones, especially at the initial 50 s. During cold start (first 25 s) the catalyst is not activated and the reaction has not started, the exhaust concentration is as the same as input. With the gas temperature upswing, the catalyst is activated and reaction starts and the exhaust concentration descents gradually. After start-up (50 s) there is a stable exhaust concentration and the transient operating of the catalytic converter is finished. The conversion efficiency is raised, and the exhaust concentration of CO could be diminished to 0.0004%. Similarly, the concentration trends of HC (Fig. 5(b)) and NO (Fig. 5(c)) are the same as CO, which proved the predictive capability of the mathematical model.

Fig. 6 shows the calculated gas temperature distribution in catalytic converter with time. At the beginning of the engine start, the temperature at the front part of converter is higher than that of the rear part. At this time, the reactions occur only in the front part and the catalytic bed has not been activated wholly. When the temperature arrives at about 500 K (after 25 s), the catalyst is activated and the temperature upswings gradually along the converter because of exothermic reaction till finally temperature are at the same value at outlet and inlet of converter.

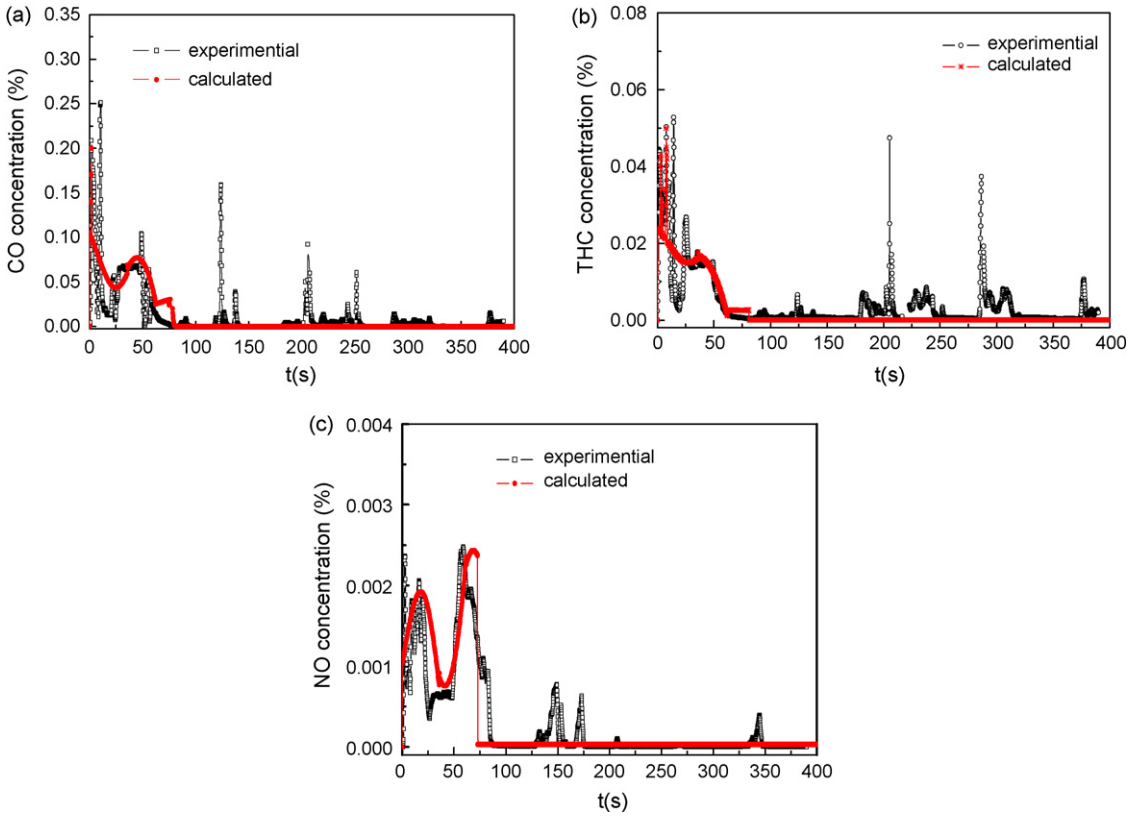

Fig. 5. Comparison of calculated concentration at catalyst output in the exhaust system with experimental data: (a) CO; (b) HC; (c) NO.

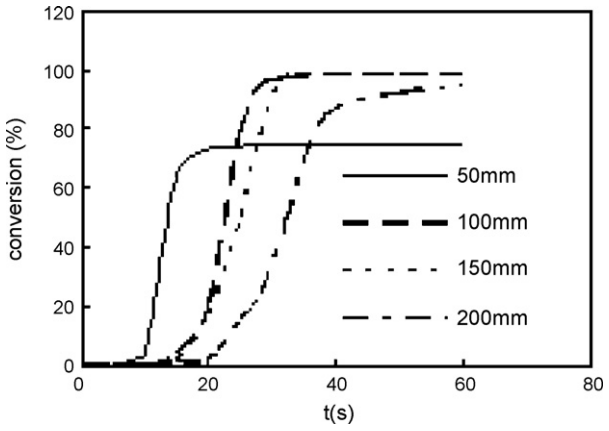

Fig. 7. The conversion of CO at different position in the converter by calculation based on kinetic model.

The temperature of the inlet gas plays an important role in light-off for the catalyst.

Fig. 7 shows the conversion of CO at different positions in the converter based on the kinetic model calculations. It is noticed that when the length of converter is 50 mm, the conversion of CO would be 78% after 15 s. When the length of converter is 100 mm, the conversion would reach 99% after 25 s. However, the conversion is only 90% after almost 40 s when the length of converter is 200 mm. This indicates that residence time and the length of converter influence the reaction efficiency considerably. This means the length of converter should be neither long nor short, the suitable length for an automobile converter is thus between 80 and 120 mm.

5. Conclusions

At present, the structure of the rate expressions proposed by Voltz et al. [14], Subramamian and Varma [15] were used in most of researches for a three-way catalystic converter. However, this proposed rate expressions must be considered as empirical and no confidence intervals in respect to the rate constants are given. They should only be used for representing monolith behavior in a reasonably narrow range of experimental conditions. Especially with the development of three-way catalyst and the high requirement of exhaust gas emission control, these expressions are limited in their applications.

In this study, kinetic data for the oxidation of CO and C_3H_6, the reduction of NO on a new catalyst developed by Kunming Sino-Platinum Metals Catalyst Co. Ltd. were determined between 500 and 700 K. The kinetic rate equations were constructed from elementary step kinetics, based upon an analysis of the reaction mechanism. The results were utilized to formulate a system of reaction rate equations and to evaluate the key kinetic parameters. A model was presented for the simulation of automobile exhaust gas converter including for the heat and mass transfer under engine cold-start condition. The calculating results are agreement with the measured data. It is indicated that the reaction mechanisms are capable to describe the behavior of automotive exhaust gas converters, the predictive capability of the model is acceptable. The light-off point of the catalytic converter reflects by the change of exhaust concentration of the main components: HC, CO and NO. The reacting temperature can be used as a guideline for catalyst light-off. Both experimental results from the synthetic gas mixtures and predictions of the kinetic model agree favorably with the observed rates of CO, C_3H_6 and NO in real engine exhausts.

Acknowledgements

Financial support for this project was provided by Yunnan Natural Science Foundation of China (2004B0028Q), National High Technology Research and Development Plan (863 of China, 2007AA06Z321), which is greatly acknowledged.

References

[1] S.T. Lee, R. Aris, On the effects of radiative heat transfer in monoliths, Chem. Eng. Sci. 32 (1977) 827–837.
[2] S.H. Oh, J.C. Cavendish, Mathematical modeling of a catalytic converter light off. Part 1 and 2, AIChE J. 31 (1985) 935–949.
[3] R.E. Hayes, S.T. Kolaczkowski, W.J. Ghomas, J. Titiloye, Finite-element model for a catalytic monolith converter, Comput. Chem. Eng. 16 (1992) 645–657.
[4] R.E. Hayes, S.T. Kolaczkowski, Mass and heat transfer effects in catalytic monolith reactors, Chem. Eng. Sci. 49 (1994) 3587–3599.
[5] C. Bruno, P.M. Walsh, D.A. Santavicca, N. Sinha, Y. Yaw, Catalytic combustion of propane/air mixtures on platinum, Combust. Sci. Technol. 31 (1983) 43–740.
[6] O. Bensalem, W. Ernst, Mathematical modeling of homogeneous–heterogeneous reactions in monolithic catalysts, Combust. Sci. Technol. 29 (1982) 1–13.
[7] S.H. Chan, D.L. Hoang, Chemical reactions in the exhaust system of a cold-start engine, Chem. Eng. Technol. 23 (2000) 727–730.
[8] S.H. Chan, D.L. Hoang, Heat transfer and chemical reactions in exhaust system of a cold-start engine, Int. J. Heat Transfer 42 (1999) 4165–4183.
[9] D.N. Tsinoglou, G.C. Koltsakis, D.K. Missirlis, K.J. Yakinthos, Transient modeling of flow distribution in automotive catalytic converters, Appl. Math. Model. 28 (2004) 775–794.
[10] C.J. Bennett, R.E. Hayes, S.T. Kolaczkowski, W.J. Thomas, An experimental and theoretical study of a catalytic monolith to control automobile exhaust emissions, Proc. R. Soc. Lond. A 439 (1992) 465–483.
[11] S. Siemund, J.P. Leclerc, D. Schweich, M. Prigent, F. Castagna, Three-way monolithic converter: simulations versus experiments, Chem. Eng. Sci. 51 (1996) 3709–3720.
[12] G.C. Koltsakis, P.A. Konstantinidis, A.M. Stamatelos, Development and application range of mathematical models for 3-way catalytic converters, Appl. Catal. B: Environ. 12 (1997) 161–168.
[13] K. Ramanathan, D.H. West, V. Balakotaiah, Optimal design of catalytic converters for minimizing cold-start emissions, Catal. Today 98 (2004) 357–373.
[14] S.E. Voltz, C.R. Morgan, D. Liederman, S.M. Jacob, Kinetic study of carbon monoxide and propylene oxidation on platinum catalysts, Ind. Eng. Chem. Prod. Res. Dev. 12 (1973) 294–301.
[15] B. Subramanlam, A. Varma, Reaction kinetics on a commercial three-way catalyst: the CO–NO–O_2–H_2O system, Ind. Eng. Chem. Prod. Res. Dev. 24 (1985) 512–516.
[16] C. Dubien, D. Schweich, Three-way catalytic converter modeling—numerical determination of kinetic data, in: Fourth Congress on Catalysis and Automotive Pollution Control, April, Brussels, Belgium, 1997, pp. 8–11.
[17] K.N. Pattas, A.M. Stamatelos, P.K. Pistikopoulos, G.C. Koltsakis, P.A. Konstandinidis, E. Volpi, E. Leeroni, Transient modeling of three-way catalytic converters, SAE Technical Paper Series 1994, 94-0934-289.
[18] S.H. Oh, G.B. Fisher, J.E. Carpenter, D.W. Goodman, Comparative kinetic studies of CO–O_2 and CO–NO reactions over single crystal and supported rhodium catalysts, J. Catal. 100 (1986) 360–376.
[19] P. Mannila, T. Salmi, H. Haario, M. Luoma, M. Harkonen, J. Sohlo, Stationary kinetics of essential reactions on automobile exhaust Pt–Rh/Al_2O_3 catalyst, Appl. Catal. B: Environ. 17 (1996) 179–198.
[20] G. Dolane, S. Strmcnik, J. Petrovcic, NO selective catalytic reduction control based on simple models, J. Process Control. 11 (2001) 35–51.
[21] J. Shi, Hand-Book of Chemical Engineering, Chemical Industry Press, Beijing, 2002, pp. 178 (in Chinese).
[22] R.B. Bird, W.E. Stewart, E.N. Lightfoot, Transport Phenomena, Wiley, New York, 1960, pp. 204.
[23] L.P. Ma, P. Ning, A.M. Zhang, Mathematical simulation of automotive exhaust catalytic converter in exhaust system of cold-start engine, J. Chem. Ind. Eng. (China) 56 (2005) 2124–2130.